

Quantum Chemical Investigation of Cluster Models for TiO₂ Nanoparticles with Water-Derived Ligand Passivation: Studies of Excess Electron States and Implications for Charge Transport in the Gratzel Cell

Vladimir Blagojevic,[†] Yiing-Rei Chen,[‡] Michael Steigerwald, Louis Brus,* and Richard A. Friesner

Department of Chemistry, Columbia University, New York, New York 10025

Received: June 6, 2009; Revised Manuscript Received: September 9, 2009

We present hybrid DFT calculations for large TiO₂ cluster models in the gas phase and in solution. Two clusters are investigated, one derived from the anatase bulk structure and the second from rutile. The surfaces are passivated with hydroxyl and water ligands, and continuum solvation is used to model bulk solvent in a subset of calculations. The geometrically optimized bonding patterns, structures, and electronic properties are similar in the two clusters. The distinction between anatase and rutile is minor at this small size. The HOMO and LUMO of the clusters are delocalized, and qualitatively resemble those observed in bulk for both the anatase and rutile derived species. When an additional electron is added, the wave function is again delocalized and there is little change in geometry, and hence minimal polaronic self-trapping. Removal of a surface ligand, creating a defect in that location, does lead to localization of the wave function, but it is unclear whether this actually occurs in real nanocrystalline TiO₂ systems. Our results suggest that modeling of electron transport in TiO₂ nanocrystal photovoltaic cells may require the presence of electrolyte ions to stabilize localized trapping states.

I. Introduction

Titanium dioxide is an important material widely used in science and technology.^{1,2} Its nanoparticles are proving to be very suitable for photochemical applications^{3–5} and interfacing with organic molecules⁶ and DNA.⁷

Although, macroscopically, the rutile phase is more thermodynamically stable than the anatase phase at ambient pressure and room temperature,⁸ anatase has been found to be easy to synthesize at the nanoscale. Banfield^{2,9,10} found that the synthesis of nanocrystalline TiO₂ consistently resulted in anatase nanoparticles, which transformed to rutile upon reaching a particular size (<14 nm). Transformation from anatase to rutile has been observed under varying experimental conditions,^{11,12} like temperature and particle size. Barnard and Zapol conducted an extensive theoretical study of TiO₂ nanostructures. They used a thermodynamic model¹³ based on the free energy of nanocrystals as a function of size and shape to determine the minimum energy morphology of anatase and rutile phases at the nanoscale and to examine the phase stability of faceted TiO₂ nanocrystals¹⁴ as a function of surface hydrogenation.¹⁵ They predicted that the minimum energy morphology of anatase is a bifrustum Wulff construction¹⁶ and that of rutile is a bitetragonal bipyramidal Wulff construction, which became more oblate as the hydrogenation level increased. They used these results to study the relative phase stability of nanoscale anatase and rutile in water¹⁷ and their surfaces with adsorbates representative of acidic and basic conditions.¹⁸ They looked at the (001), (100), and (101) surfaces of anatase and the (100), (011), and (110) surfaces of rutile, as these are the most common crystalline planes in bulk crystals and nanoparticles alike.

In recent years, TiO₂ has attracted attention as a material for dye-sensitized solar cells.^{19–21} It was found that the use of TiO₂ nanocrystals improves solar cell efficiency. There has been extensive investigation in the process of electron injection into the nanoparticles by the light-absorbing dye.²² Potential existence of defects on the nanocrystal surface, like oxygen vacancies, represents an additional dimension to this problem. Experimental studies have shown that oxygen vacancies in rutile can act as active sites for water dissociation²³ and bonding sites for molecules and metal clusters.²⁴

Our principal focus in the present paper is on understanding key electronic states (e.g., anionic states containing an excess electron) of TiO₂ nanoparticles, via density functional theory (DFT) calculations, in the condensed phase environment characteristic of photovoltaic devices such as the Gratzel cell. The preparation of the nanoparticles invariably involves some exposure to water, and it is believed that this results in passivation of the surface by water-derived ligands, e.g., water itself or hydroxyl. The remainder of the solution phase environment is modeled via dielectric continuum theory, using standard quantum chemical self-consistent reaction field techniques. The deployment of this environment and the focus on the electronic structure of the anion and possible trapping states for the excess electron differentiate the present paper from previous DFT calculations on TiO₂ nanoparticles.^{31–33}

We begin by constructing passivated cluster models for both anatase and rutile derived nanocrystals. We find that the anatase and rutile model clusters show quite similar surface structure, which in fact is different than either the anatase or rutile bulk structures. However, even in our small model clusters of 21–23 titanium atoms, the delocalized lowest unoccupied molecular orbitals (LUMOs) are very similar to those of the bulk anatase and rutile band structures, respectively. The oxygen centered highest occupied molecular orbital (HOMO) is delocalized in

[†] Present address: Chemistry Department, University of Waterloo, Waterloo, Ontario, Canada.

[‡] Present address: Physics Department, National Taiwan Normal University, Taipei 11677, Taiwan.

both anatase and rutile model clusters, while the d-band LUMO is delocalized in anatase and localized in a plane in rutile. Removal of a water ligand from the surface of a model rutile cluster led to increased localization of the LUMO near this site.

As a next step, we add an excess electron and carry out calculation in both vacuum and continuum solvent environments. We examine what happens to the excess electron as a function of environment and also in the absence and presence of a defect site created by removing a passivation ligand. Unless a defect is created, we do not see significant localization of the excess electron, although the delocalization patterns are, interestingly, different for the rutile and anatase nanocrystal models.

The paper is organized as follows. In section II, we briefly describe the quantum chemical computational methods. Section III presents the results obtained for both the anatase and rutile clusters. In section IV, we summarize our results, and discuss the implications for the TiO₂ nanoparticle systems of the Gratzel cell and other solar energy conversion devices. Our calculations tentatively suggest that other important system components, such as electrolyte ions, play a key role in the quantitative electron transport. The work described here provides a starting point for investigating larger, more complex models.

II. Computational Methodology

It is important to use methods that are known to quantitatively reproduce a diverse range of chemical bonding situations in finite structures with real surfaces. We use a real space, atom-centered basis and a hybrid functional in density functional theory (DFT) that combines exact Hartree–Fock exchange with the generalized gradient approximation. Hybrid functionals reproduce experimental bond energies and ionization potentials in a standard test set of small molecules with residual errors of 0.13 eV, about 10% of the residual errors found for the commonly used local density approximation (LDA).^{14,15} Hybrid functionals also give an improved band structure and band gap for semiconductors such as crystalline Si in comparison to LDA.¹⁶ The improvement for complex crystalline oxides such as La₂CuO₄, CaCuO₂, LaMnO₃, Cr₂O₃, NiO, TiO₂, and UO₂ is dramatic; in these oxides, LDA often gives qualitatively incorrect (metallic) results.^{16,17} Overall, the accuracy and utility of hybrid functionals is being established through widespread application.¹⁸ We use the B3LYP hybrid functional.¹⁴

The static DFT calculations were performed on personal computers using the Jaguar 6.0 code.¹⁹ Complete geometric optimization of species with up to about 200 atoms can be done. We do not assume any symmetry. Calculations were done with an all-electron 6-31g basis for the O and H, and pseudopotentials with the LACVP basis for Ti atoms.²⁰ Extensive tests on model small molecules, which will be described elsewhere, show that this basis set is sufficient to describe geometries quantitatively and energetics at a semiquantitative level, which is the goal of the present study. Future work will employ larger basis sets which are required for highly accurate energetics. Spin–orbit effects are not included in our calculations. In the case of some ionized species, we reoptimized the structure in the presence (or absence) of the extra charge, in order to understand changes in the doped nanocrystal geometry as a function of charge state. The vertical ionization potential (electron affinity) is the total energy difference when the ion is converged for the fixed geometry of the neutral. The adiabatic ionization potential (electron affinity) is the energy difference when the ion is also geometrically optimized. The average of the ionization potential and electron affinity gives the electron chemical potential while the difference between them is the chemical hardness, corresponding to an effective charging energy.

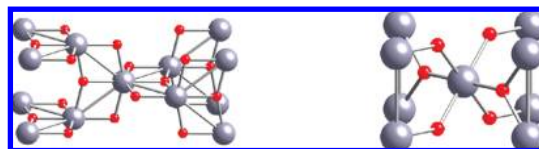


Figure 1. Anatase (left) and rutile (right) unit cells. Oxygen atoms are red.

In order to improve our understanding of behavior of TiO₂ nanocrystals in solution, we used the continuum solvation model available in the Jaguar 6.0 code. In this type of calculation, the solvated system is treated with a self-consistent reaction field method, using Jaguar's Poisson–Boltzmann solver.^{25,26} The process consists of Jaguar first solving the usual gas phase wave function and, from that, the electrostatic potential, and fitting that potential to a set of atomic charges. These charges are used by the Poisson–Boltzmann solver, which determines the reaction field by numerical solution of Poisson–Boltzmann equations and represents the solvent as a layer of charges at the molecular surface (which serves as a dielectric continuum boundary). These solvent point charges are then incorporated into another quantum mechanical wave function calculation. The process is repeated until self-consistency is obtained. Solvated calculations of various neutral and ionic nanocrystals are presented below, along with gas phase results.

III. Results

Ti has four valence electrons and is six coordinate in TiO₂. There are two types of Ti–O bonds in the bulk crystals: short (1.934 Å in anatase, 1.947 Å in rutile) and long (1.98 Å in both anatase and rutile). We consider the Ti bonding as a combination of four covalent and two dative bonds. We model the electronic structure of small prototypical clusters based on anatase and rutile in an aqueous environment at neutral pH.

The basic structural unit of both anatase and rutile is a distorted TiO₆ octahedron. The two long dative bonds are axial in both structures. The O atoms forming these axial bonds are also bonded covalently to two Ti atoms, as shown in Figure 1. In rutile, these two OTi₂ moieties are coplanar, and in anatase, the planes are rotated 90° with respect to each other. An analogous structural distinction would occur in the small model complex *trans*-Ti(OH)₄(OH₂)₂ which has similar covalent and dative Ti bonding. In the rutile isomer, the two H₂O are coplanar, and in the anatase isomer, the two H₂O are rotated at 90°.

Our two initial model clusters were chosen to have the interior structure of anatase and rutile. The surface planes were chosen to match the respective Wulff shapes: (101) and (001) planes for anatase and (110) and (101) planes for rutile. Surface Ti atoms are terminated using covalent –OH groups and dative water molecules. Thus, all of the titanium atoms are kept tetravalent and hexacoordinate. Initially, the two clusters were optimized in vacuum, and the effect of continuum water solvation was then considered.

Our initial rutile cluster converged as shown in Figure 2, with relatively small geometry changes. Our initial anatase cluster, on the other hand, fragmented in geometrical optimization, often creating a more open 2D-like structure with some double Ti–O bonds. We then abandoned the Wulff shape for anatase, and began with a more compact reactangular structure which did converge.

In both the anatase-inspired Ti₂₁O₇₀H₅₄ cluster and the rutile-inspired Ti₂₃O₈₀H₆₈ cluster, the central titanium atom (highlighted yellow in Figure 2) is bulk-like. All other titanium atoms

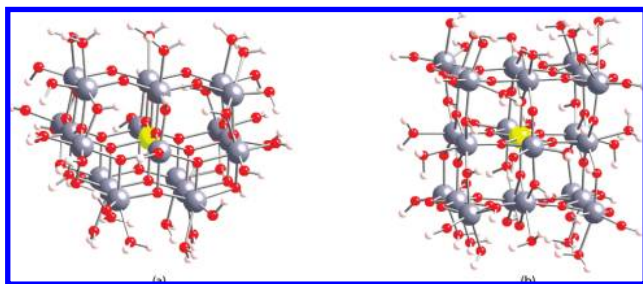


Figure 2. Optimized geometries: (a) anatase $\text{Ti}_{21}\text{O}_{70}\text{H}_{54}$; (b) rutile $\text{Ti}_{23}\text{O}_{80}\text{H}_{68}$.

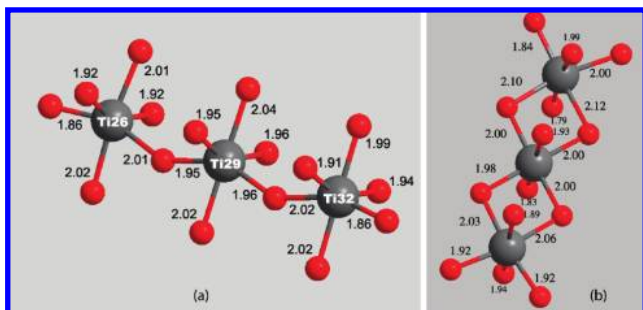


Figure 3. Central chain of titanium atoms in anatase (a) and rutile (b) clusters with corresponding Ti–O bond lengths. The middle Ti atom is the central Ti atom of each nanocrystal.

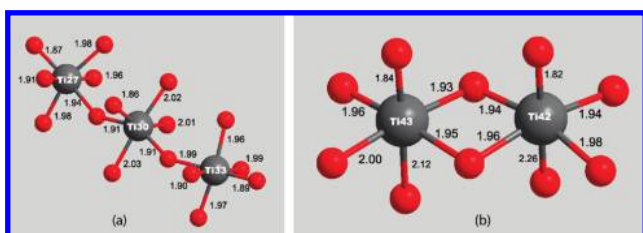


Figure 4. Side chain of titanium atoms in anatase (a) and rutile (b) clusters with corresponding Ti–O bond lengths.

are on the surface. The four sides of the rectangular rutile cluster are (110), while the back and the front are (001). The (001) plane is present because of the small size of the cluster, which does not have enough room to for the expected (101) plane. The top and bottom plane in our anatase cluster is (001), while the (101) plane, which is prominent in the bulk, does not even appear. The anatase cluster is actually too small to contain one bulk unit cell in the direction of the axial bonds, as can be seen by comparing the cluster model and the bulk unit cell.

These anatase and rutile clusters, rectangular in shape, can be considered as composed of three types of titanium dioxide chains: central, side, and edge. The central chain (Figure 3) contains the central titanium atom; it is surrounded on all four sides with other chains, and its surface is limited to the terminal groups at its ends. Side chains (Figure 4) have one of their sides exposed, in addition to the ends of the chain, meaning they represent, roughly, the typical feature of the surface of any anatase and rutile structure. Edge chains (Figure 5) have two of their sides exposed; they include corner atoms and represent a feature that would be characteristic of nanocrystals. There are two different edge chains in our anatase cluster due to the limitations in cluster size.

In both anatase and rutile clusters, the central titanium atom (Figure 3) has four roughly equivalent bonds in the equatorial plane (1.95–1.96 Å in anatase, 1.98–2.00 Å in rutile) and two bonds on the axis, which are longer than equatorial bonds in

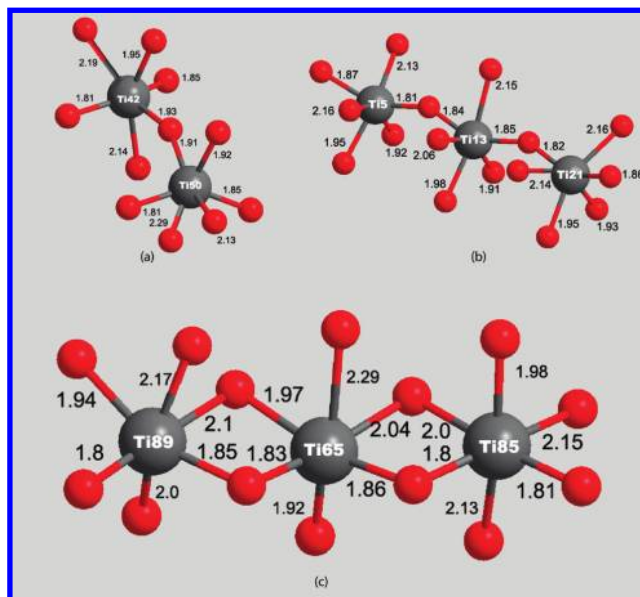


Figure 5. Edge chains of titanium atoms in anatase (a, b) and rutile (c) clusters with corresponding Ti–O bond lengths.

anatase (2.02–2.04 Å) and shorter in rutile (1.83, 1.93 Å). We note that the bond arrangement around the central titanium atom in the anatase cluster corresponds closely to that of bulk anatase, while the same is not true for the rutile cluster.

The surface titanium atoms (Figures 4 and 5) in both anatase and rutile clusters can generally be described as having a cis orientation of long or short bonds. The number of long bonds is two or three. A third long bond is usually accompanied by a short bond in trans orientation with respect to one of the long bonds. Ti–O bonding varies with the type of oxygen coordination: in 3-coordinated oxygen atoms, the bond lengths are distributed typically as one long (~ 2.1 Å) and two short (~ 1.9 Å) bonds; in 2-coordinated oxygen atoms, there are two short bonds of different length: one 1.76–1.78 Å and the other 1.86–1.90 Å. The atoms that have water coordinated to them have another long bond (2.03–2.17 Å) in the cis position with respect to water. Interestingly, these bonding patterns occur in the same manner in both the anatase and rutile clusters. In addition to this, we can see some correlation between terminal Ti–OH bond length and terminal Ti–O–H angle. Typically, short bonds (1.78–1.82 Å) correspond to a bigger than normal angle (170–140°), while longer bonds (1.92–2.1 Å) have angles in the range 115–125°. In addition, longer terminal Ti–OH bonds correspond to shorter complementary (located trans with respect to titanium atom) bridging Ti–O bonds, and vice versa. The similarity in local structure between anatase and rutile was not initially present but developed during the process of geometrical optimization.

The cluster structure discussed so far refers to vacuum. In order to model the effect of water, we added an artificial dielectric environment to our calculations. The presence of water solvent decreases the length differences in the surface bonds. The shorter bonds lengthened and the longer bonds shortened, so that the differences were about one-half those in vacuum. In addition, the absolute atomic charges from Mulliken population analysis increased when we introduced artificial solvation, making titanium atoms more positive and oxygen atoms more negative. The polar water solvent makes the bonding more ionic in both isomers.

Figure 6 shows the charging behavior of the total electronic energy in vacuum; here also, the two clusters are similar. Both

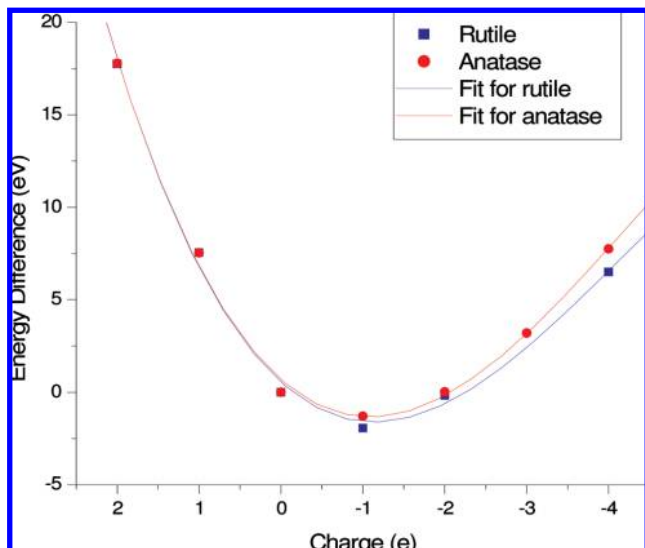


Figure 6. Total energy dependence on cluster net charge for fixed optimized neutral geometry in vacuum. Energies are relative to the energy of the neutral cluster.

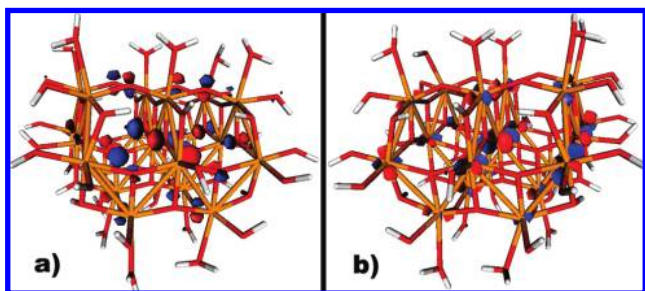


Figure 7. HOMO (a) and LUMO (b) of the anatase cluster.

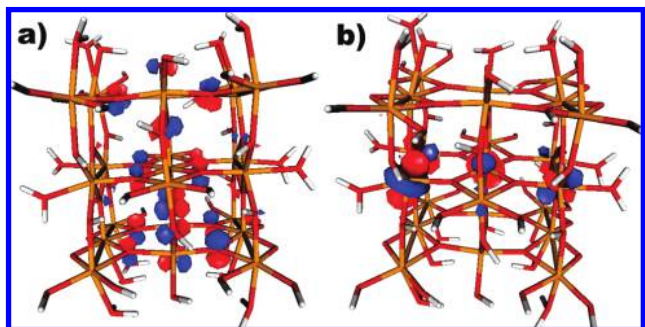


Figure 8. HOMO (a) and LUMO (b) of the rutile cluster.

show positive vertical electron affinities; the rutile value is slightly higher. The dependence of total energy (relative to the energy of the corresponding neutral nanocrystal) on charge is well represented by a polynomial curve of third order. The second order coefficient is the chemical hardness η ,²⁷ and it predicts effective capacitance C in the relation $\eta = e^2/C$. The two capacitances, as well as the two electron chemical potentials, are almost the same.

The HOMO–LUMO gap in the anatase cluster is 3.85 eV; in the rutile cluster, the gap is 3.91 eV. In both anatase and rutile, the neutral HOMO is delocalized across the entire cluster. It is centered almost entirely on the bridging oxygen atom p-orbitals, similar to the valence band in bulk TiO₂. The electron density is highest at the center of the cluster, as would be expected from effective mass theory for an S orbital. The LUMO orbitals are somewhat different in the two clusters. In the anatase

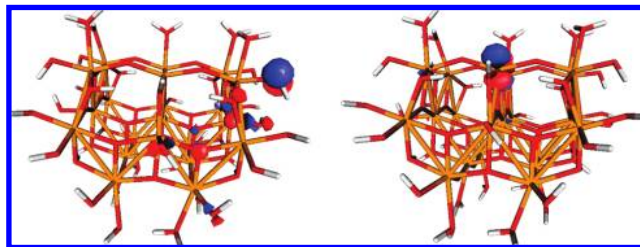


Figure 9. HOMO (left) and LUMO (right) of the anatase cluster with one water molecule removed calculated using the fixed geometry of the fully coordinated cluster.

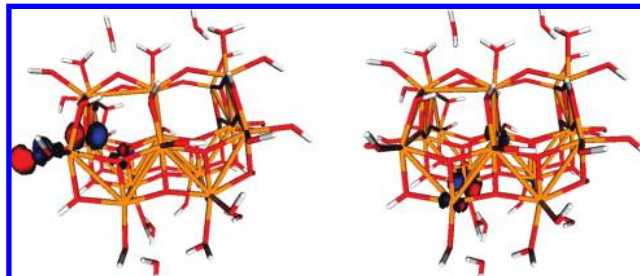


Figure 10. HOMO (left) and LUMO (right) of the anatase cluster with one water molecule removed calculated with full geometrical optimization. Note when one water is removed from the ligand shell, the cooperativity in the binding is partially disturbed and multiple ligands dissociate. This subject will be further explored.

cluster, the LUMO is delocalized across the cluster, residing on the Ti d-orbitals in agreement with the bulk conduction band. The orbital density is highest on the central plane, which contains the majority of titanium atoms, and it is reduced on two other planes, above and below the central plane. The density does not vary significantly among titanium atoms in the same plane.

In contrast, in the rutile cluster, the d-orbital LUMO is localized almost entirely on the central plane. The orbital density is symmetric and increased at the sides of the cluster. This pattern does not change with the inclusion of the aqueous artificial solvation to the calculation. The bulk anatase conduction band has high dispersion in the z -direction and much lower dispersion in the x – y plane. Thus, in our anatase cluster, the observed localization on the central plane and increased density at the side chains make sense in this context.

In the geometrically optimized anions, the half-filled state is in the band gap, 3.46 and 3.04 eV above the valence band and 0.89 eV and 0.809 eV below the conduction band in anatase and rutile, respectively. The LUMO of the neutral cluster is very similar to the orbital occupied by the extra electron in the geometrically optimized anion. That is, there is no self-trapping; the extra electron in both anatase and rutile clusters does not alter the geometry in any significant way upon reoptimization. The conduction band in the bulk rutile phase is relatively flat along the (110) direction; thus, it appears that the localization in one of the (110) planes is intrinsic. In anatase, the orbital is delocalized across titanium centers, which is in agreement with the bulk anatase band structure.

When a single water molecule is removed from one Ti on the surface, the clusters respond differently, with modest changes in both geometrical and electronic structure. By comparing the frozen (Figure 9) and fully optimized anatase cluster with one water removed (Figure 10), we observe shifts in the position of both the HOMO and LUMO. The HOMO shifts from one side of the cluster to the other, while the LUMO shifts from the site of the removed water molecule in frozen geometry to the furthest

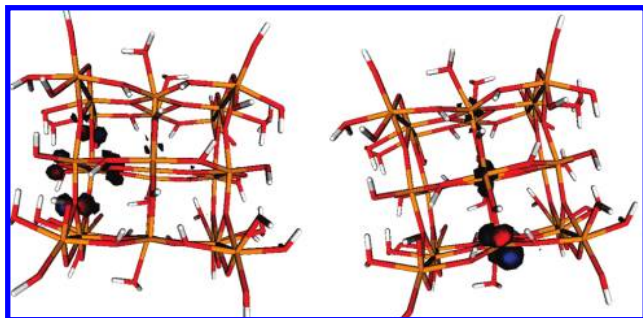


Figure 11. HOMO (left) and LUMO (right) of the rutile cluster with one water molecule removed calculated using the fixed geometry of the fully coordinated cluster.

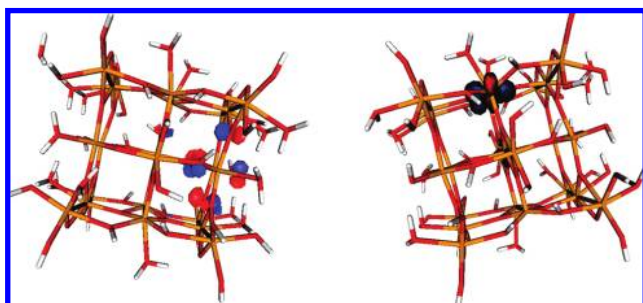


Figure 12. HOMO (left) and LUMO (right) of the rutile cluster with one water molecule removed calculated with full geometrical optimization.

plane away from this defect. Band gaps are 4.14 eV for frozen geometry and 4.53 eV for optimized cluster. Ionization potentials are 6.54 eV for frozen and 6.86 eV for optimized geometry.

In the rutile cluster, the HOMO remains unchanged during the optimization process (left images in Figures 11 and 12). The LUMO shifts from the position at the site of the removed water molecule (Figure 11, right) to the plane on the opposite side of the cluster (Figure 12, right). The optimized cluster is more stable by 0.91 eV. The band gaps are 3.72 eV in frozen and 3.86 eV in optimized cluster, while ionization potentials are 6.83 eV in the frozen and 6.90 eV in the optimized geometry. The energy difference between the LUMO and LUMO+1 is 0.06 eV in the frozen and 0.18 eV in the optimized cluster.

IV. Discussion and Conclusion

The geometrical optimization energy change is much larger in the anatase cluster (6.7 eV) than in the rutile cluster (0.9 eV). In addition, the differences in band gap energies and ionization potentials of frozen and optimized clusters with a missing water molecule are larger in the anatase cluster than in the rutile cluster. Thus, the anatase-inspired cluster undergoes a larger change in electronic structure during the geometry optimization process than the rutile-inspired one. The two different initial clusters evolve toward one common structure mostly dominated by the surface passivated with $-OH$ and water ligands. At this small size, the difference between anatase and rutile in electronic properties is nearly lost after optimization. In this regard, recall that the anatase cluster is actually too small to contain a complete anatase structural unit along the central Ti atom axial bonds. The optimized surface structures of both clusters are very similar, in the sense that their local bonding resembles neither bulk anatase nor bulk rutile.

Around the central Ti atom, a remnant of the difference between anatase and rutile remains. In the anatase cluster, the central titanium atom local structure closely resembles bulk

anatase. In the rutile nanocrystal, however, the central atom local structure is different than that of bulk rutile, with two short and four long bonds, as opposed to two long and four short bonds in the bulk structure. The fact that the distortions with respect to bulk bonding decrease with introduction of artificial dielectric around the nanocrystals suggests that the distortions of both anatase and rutile clusters are probably the result of the system trying to establish optimal covalent bonding around titanium atoms, moving toward a more tetrahedral orientation of the Ti–O covalent bonds. This is offset by the constraints of the internal lattice of the respective crystal systems, resulting in a balance between distortion on the surface and bulk-like three-dimensional structure in the interior.

The results we have obtained in principle depend upon many aspects of the calculations and physical model. Further exploration of many of these factors will be necessary to establish the key conclusions as robust. Some of the important directions to explore include performing calculations with increased basis set size (e.g., adding polarization functions to the oxygen), systematically increasing the size of the cluster, and investigating the effects of using a different DFT functional. Additionally, an investigation of different types of surface structures would be useful. For example, Rajh, Zapol, and co-workers have suggested the importance of Ti=O surface groups. Such groups are likely to react with water, and thus, we did not include them in this present manuscript. The stability of such structures as compared to passivation by water-derived ligands, in an environment where such ligands are present in significant concentrations, could be addressed by suitable calculations. We intend to pursue new calculations along these lines as a follow-up to the present study.

The presence of a defect site (missing water molecule from the coordination sphere) on the surface of both anatase and rutile clusters causes changes to the LUMO in similar fashion: in both clusters, in fully optimized geometry, the LUMO is localized on the site on the opposite side of the cluster with respect to the site of the defect. Calculation using the frozen structure of the fully optimized, fully coordinated cluster reveals that this localization is caused by the geometrical optimization of the defect clusters: the LUMO is localized at the site of the defect in frozen geometry and moves away when the optimization is completed. This is very interesting, because it might indicate that the surface defects relating to the coordination sphere of the titanium atoms (molecules with donor–acceptor bonds to titanium) in both anatase and rutile do not create surface traps for injected electrons.

In conclusion, we have used the accumulated information to construct two nanocrystals: anatase-inspired $Ti_{21}O_{70}H_{54}$ and rutile-inspired $Ti_{23}O_{80}H_{68}$. We conducted geometrical optimization of these clusters, and the analysis of the optimized geometry has shown that, in terms of the short-range environment around individual titanium centers on the surface, both clusters exhibit similar structure, which is different from both bulk anatase and rutile. This distortion appears to have little or no effect on the interior titanium atom in anatase nanocrystal, while the interior titanium atom in rutile nanocrystal shows significant distortion from bulk structure. The cluster HOMOs and LUMOs correspond well to the conduction and valence bands of the bulk anatase and rutile.

These results leave open the question of the nature of the trap states in TiO_2 nanocrystals that are thought to be responsible for slow electron diffusion in devices such as the Gratzel cell. When the surface of our model cluster is fully passivated, no localized states are observed. Removal of a water molecule can

lead to localization, but one has to question how likely this is in an environment that has a significant ligand concentration. Other types of structural defects are possible, but it is again not obvious what their concentration or energetics would be.

A likely possibility suggested by these preliminary studies is that the positive ions of the electrolyte are involved in transport and trapping in an integral fashion. The involvement in transport has already been suggested by a decade of experimental results,²⁸ among other observations, the Grätzel cell requires a very high electrolyte concentration to function at all. Recent work by Frank and co-workers^{29,30} suggests that the trapping states lie on the surface of the particle. If this is indeed the case, one can imagine an interaction of the positive ions of the electrolyte with surface oxygens leading to a temporarily stabilized structure which can accommodate the centroid of the wave function of a negative charge. Such states can be created transiently as the electron moves through the material. Testing this hypothesis will require building models that incorporate the ionic liquid environment, via either continuum models or explicit solvent simulations.

Acknowledgment. This work was supported by grants from the DOE to R.A.F. (DE-FG02-90ER14162) and L.B. (DE-FG02-98ER14861). It was also supported by the NSF through the Columbia MRSEC (DMR-0213574) and by the New York State Office of Science, Technology and Research (NYSTAR). We thank Mark Hybertsen for extensive discussions during the early stages of this work.

References and Notes

- (1) Elder, S. H.; Cot, F. M.; Su, Y.; Heald, S. M.; Tyrshkin, A. M.; Bowman, M. K.; Gao, Y.; Joly, A. G.; Balmer, M. L.; Kolwaite, A. C.; Magrini, K. A.; Blake, D. M. *J. Am. Chem. Soc.* **2000**, *122*, 5138.
- (2) Zhang, H.; Banfield, J. *J. Mater. Chem.* **1998**, *8*, 2073.
- (3) Zhang, W. F.; Zhang, M. S.; Yin, Z.; Chen, Q. *Appl. Phys. B* **2000**, *B70*, 261.
- (4) Thomas, A. G.; Flavell, W. R.; Kumarasinghe, A. R.; Mallick, A. K.; Tsoutsou, D.; Smith, G. C.; Stockbauer, R.; Patel, S. *Phys. Rev. B* **2003**, *67*, 35110.
- (5) Persson, P.; Bergström, R.; Ojamäe, L.; Lunell, S. *Adv. Quantum Chem.* **2002**, *41*, 203.

- (6) Rajh, T.; Chen, L. X.; Lukas, K.; Liu, T.; Thurnauer, M. C.; Tiede, D. M. *J. Phys. Chem. B* **2002**, *106*, 10543.
- (7) Paunesku, T.; Rajh, T.; Wiederrecht, G.; Maser, J.; Vogt, S.; Stojicevic, N.; Protic, M.; Lai, B.; Oryhon, J.; Thurnauer, M.; Woloschak, G. *Nat. Mater.* **2003**, *2*, 343.
- (8) Muscat, J.; Swamy, V.; Harrison, N. M. *Phys. Rev. B* **2002**, *65*, 224112.
- (9) Gribb, A. A.; Banfield, J. F. *Am. Mineral.* **1997**, *82*, 717.
- (10) Zhang, H. Z.; Banfield, J. F. *J. Phys. Chem. B* **2000**, *104*, 3481.
- (11) Gourma, P. I.; Mills, M. J. *J. Am. Ceram. Soc.* **2001**, *84*, 619.
- (12) Li, Y.; White, T.; Lim, S. H. *Rev. Adv. Mater. Sci.* **2003**, *5*, 211.
- (13) Barnard, A. S.; Zapol, P. *J. Chem. Phys.* **2004**, *121*, 4276.
- (14) Barnard, A. S.; Zapol, P. *Phys. Rev. B* **2004**, *70*, 235403.
- (15) Barnard, A. S.; Zapol, P. *J. Phys. Chem. B* **2004**, *108*, 18435.
- (16) Wulff, G.; Kristallogr. *Z. Mineral* **1901**, *34*, 449.
- (17) Barnard, A. S.; Zapol, P.; Curtiss, L. A. *J. Chem. Theory Comput.* **2005**, *1*, 107.
- (18) Barnard, A. S.; Zapol, P.; Curtiss, L. A. *Surf. Sci.* **2005**, *582*, 173.
- (19) Grätzel, M. *Nature* **2001**, *414*, 338.
- (20) Grätzel, M. *J. Photochem. Photobiol., A* **2004**, *164*, 3.
- (21) Wang, P.; Klein, C.; Humphry-Baker, R.; Zakeeruddin, S. M.; Grätzel, M. *Appl. Phys. Lett.* **2005**, *86*, 123508.
- (22) Tachibana, Y.; Nazeeruddin, M. K.; Grätzel, M.; Klug, D. R.; Durrant, J. R. *Chem. Phys.* **2002**, *285*, 127.
- (23) Schaub, R.; Thosttrup, P.; Lopez, N.; Lægsgaard, E.; Stensgaard, I.; Nørskov, J. K.; Besenbacher, F. *Phys. Rev. Lett.* **2001**, *87* (26), 266104.
- (24) Wahlström, E.; Lopez, N.; Schaub, R.; Thosttrup, P.; Rønnow, A.; Africh, C.; Lægsgaard, E.; Nørskov, J. K.; Besenbacher, F. *Phys. Rev. Lett.* **2003**, *90* (2), 26101.
- (25) Tannor, D. J.; Marten, B.; Murphy, R.; Friesner, R. A.; Sitkoff, D.; Nicholls, A.; Ringnalda, M.; Goddard III, W. A.; Honig, B. *J. Am. Chem. Soc.* **1994**, *116*, 11875.
- (26) Marten, B.; Kim, K.; Cortis, C.; Friesner, R. A.; Murphy, R. B.; Ringnalda, M. N.; Sitkoff, D.; Honig, B. *J. Phys. Chem.* **1996**, *100*, 11775.
- (27) Zhou, Z.; Steigerwald, M.; Hybertsen, M.; Brus, L.; Friesner, R. A. *J. Am. Chem. Soc.* **2004**, *126*, 3597.
- (28) Frank, A. J.; Kopidakis, N.; van de Lagemaat, J. *Coord. Chem. Rev.* **2004**, *248*, 1165–1179.
- (29) Zhu, K.; Kopidakis, N.; Neale, N. R.; van de Lagemaat, J.; Frank, A. J. *J. Phys. Chem. B* **2006**, *110* (50), 25174.
- (30) Kopidakis, N.; Neale, N. R.; Zhu, K.; van de Lagemaat, J.; Frank, A. J. *Appl. Phys. Lett.* **2005**, *87* (20), 202106S.
- (31) Barnard, A. S.; Erdin, S.; Lin, Y.; Zapol, P.; Halley, J. W. *Phys. Rev. B* **2006**, *73* (20), 205405.
- (32) De Angelis, F.; Fantacci, S.; Selloni, A. *J. Am. Chem. Soc.* **2004**, *126* (46), 15024.
- (33) Persson, P.; Gebhardt, J.; Lunell, S. *J. Phys. Chem. B* **2003**, *107* (15), 3336.

JP905332Z